Modeling source-source and source-filter acoustic interaction in birdsong

Rodrigo Laje* and Gabriel B. Mindlin
Departamento de Física, FCEN, Universidad de Buenos Aires, Pabellón I, Ciudad Universitaria (C1428EGA), Buenos Aires, Argentina
(Received 5 May 2005; published 27 September 2005)

We present a simple model for birdsong production in Oscine songbirds that allows us to study the acoustic interaction between their two sound sources, as well as the acoustic coupling between sources and vocal tract. This model allows us to study complex phenomena in which the traditionally assumed source-filter separation hypothesis does not hold. We make testable hypotheses about the source of complexity in the song of some birds.

DOI: 10.1103/PhysRevE.72.036218 PACS number(s): 05.45.−a, 87.19.−j, 43.80.+p, 02.30.Ks

I. INTRODUCTION

Oscine songbirds are known for their vocal learning abilities. Song learning has striking parallels to speech acquisition: both birds and humans must hear the sounds of tutors during a sensitive period and must hear their own voice during a sensorimotor period [1]. These fundamental similarities and some advantages (repetitive and easily recorded behavior, small number of neural nuclei involved, small number of muscles involved) make birdsong learning a model system for general sensory and motor learning [1,2]. Much of these studies are focused on the neural control of these processes. Yet the actual phenomenon (song production) involves the interaction between the nervous system and a physical system. Since the avian vocal organ is a nonlinear device [3], its response to the instructions sent by the nervous system can be highly nontrivial. Some of these effects are the focus of this work.

The basic mechanism of sound production in songbirds is very similar to that used by humans to generate voiced sounds in normal speech. Like the larynx in humans, the avian vocal organ (the *syrinx*) generates sound through the airflow-induced oscillation of small tissue masses called the *labia*. This oscillation modulates in turn the airflow, giving rise to an acoustic disturbance that propagates along the tract. In Oscine songbirds the syrinx is a bilateral structure located at the junction of bronchi and trachea [4]. It consists of two separate valves (one in each bronchus) capable of vibrating independently, which to some extent are also independently controlled [5]. Some birds use only one valve for singing, but some use both valves either alternatively or simultaneously [6].

Until recent years, research in birdsong was mainly concerned with the unveiling of the basic physical mechanisms responsible for the acoustic output of the syrinx, either in Oscines [7] and non-Oscines [8,9]. Recent theoretical efforts at modeling [10,11] helped to start building a bridge between neural instructions and song [12] and were experimentally validated [13]. However, a good deal of basic questions on the production of sound remain open, especially with respect to sounds displaying complex features like frequency jumps, period doubling, and subharmonic frequencies (see Fig. 1) and phenomena like source-source interactions, etc. This work builds on previous efforts [10,11] and aims at identifying possible dynamical origins of complex sonograms in Oscines. By exploring these solutions we show that the genesis of some complex acoustic features is not to be tracked to the nervous system but to the peripheral system.

A mechanism by which the avian vocal organ adds complexity to the sound was explored in the framework of the two-mass model of the labia [3]. The model showed a qualitatively similar behavior to that of *in vivo* and *in vitro* syringeal oscillations, with period-doubling bifurcations and transitions from periodic to nonperiodic dynamics. As in the case of birds, complex vocalizations in human normal speech were mainly supposed to be generated by intrinsic nonlinear dynamics in the vibration of the mechanical apparatus [15].

However, mobile tissues in the vocal organ can present irregular oscillatory behavior even disregarding complex labium structure. This can happen, for instance, if acoustic feedback is considered [16]. A common assumption in the field is the independence of the dynamics of the sound source from that of the pressure wave in the vocal tract, what is known as the *source-filter separation hypothesis*. Under this assumption, the sound generation problem is highly sim-

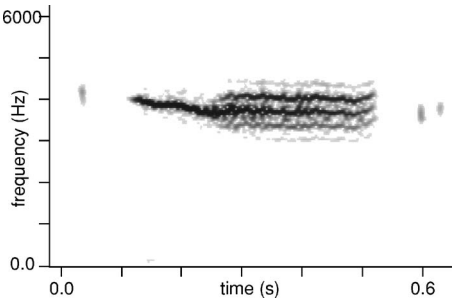

FIG. 1. A syllable of the grassland sparrow's song (*Ammodramus humeralis*) [14]. Subharmonic frequencies (appearing as sidebands) are born in a bifurcation around 0.25 s. It might be instead that a sudden change in the fundamental frequency occurs, from around 3900 Hz (the single stroke) to around 325 Hz (the difference between adjacent strokes), but such a low frequency is very unlikely in this 10-cm-long bird.

*Corresponding author. Electronic address: rodrigo@df.uba.ar

plified: the vocal tract only filters a spectrally rich signal generated by the vocal source and cannot affect the dynamics of the source. On the other hand, the sound emerging from interacting source and tract is richer, more complex, yet mathematically it is a rather involved problem. For this reason, most studies focus on the regimes where the source-filter separation hypothesis holds.

Recently, source-filter separation was experimentally demonstrated in pure-tone dove vocalizations by Beckers *et al.* [17], but there are no experimental results regarding this for complex vocalizations and there is no reason to assume it *a priori* in those cases. Indeed, the source-tract interaction was theoretically shown to be a possible dynamical origin of complexity in the vocal organ [16]. The source-tract interaction through acoustic feedback was first proposed in a model for the human vocal folds [16], showing that a very simple (two-dimensional) model of the isolated source can display complex dynamics when source and tract interact. The reason for which this issue is important is that the interaction between source and filter is a plausible mechanism by which the avian vocal organ achieves the capacity to generate complex sounds with simple neural instructions, providing a beautiful example of the deep interaction between neural system and body.

A concept associated to the source-filter separation hypothesis is that of *impedance* [18]. In this framework the vocal tract is considered a passive, linear system and therefore can be represented by its impedance, which is the ratio of (complex) acoustic pressure to particle velocity. However, this ratio is well defined only for a linear system (e.g., the vocal tract alone). In general, the vocal system is no longer linear when source and tract interact, due to the nonlinear processes that occur at the source.

In addition to labium structure and source-tract coupling, the interaction between the two sound sources is also a possible dynamical origin of complexity. The source-source interaction was first reported and experimentally demonstrated by Nowicki and Capranica [19] in the call of the Black-capped Chickadee (*Parus atricapillus*). Acoustic and structural couplings (for instance, involving the cartilaginous pessulus to which labia on both sides of the syrinx are attached) were considered. The physical mechanism responsible for such interaction, however, was speculative.

In this work we present a model for birdsong production in Oscine songbirds that allows us to study source-source and source-tract acoustic interactions. In order to achieve our goal, we separate the sources of complexity: we develop a model for labial oscillation involving a small number of spatial modes. Based on previous works, a two-dimensional model is developed in Sec. II for the single, isolated source. In Sec. III we approximate nonlinear terms in this simple model to get an even simpler form. Coupling between source and tract is treated in Sec. IV, where a more general approach than the impedance approach is discussed, and an expression for the coupling is developed. In Sec. V the complete model for two sources coupled to a tract with feedback is presented. A further approximation related to the coupling strength is made, in order to obtain a much simpler version of the complete model. Some of the solutions of this model are illustrated in Sec. VI, where testable hypotheses concerning the dynamical origin of complexity in birdsong are made and simple experiments proposed. Finally, Sec. VII contains our conclusions.

II. EXTENDED FLAPPING MODEL

Based on recent experiments by Goller, Suthers, and Larsen [5,7,20,21], an "extended flapping model" for labial oscillation in songbirds was proposed [11]. This model was built on a previous model by Titze [22], which was first proposed to account for the oscillation of human vocal folds. Titze's model is based on the experimental observation of an upward-propagating wave in the surface of the vocal fold [22,23], typically referred to as a phase difference between upper and lower portions of the fold. This wave is coupled to the oscillation of the center of mass of the fold in such a way that a "flapping" motion is realized, which allows a net energy transfer from the airflow to the fold oscillation. This flapping motion is consistent with recent videography of the avian vocal organ [3,21].

The extended flapping model was first developed to account for large amplitude oscillations of the human vocal folds [16], and then a simplified version was proposed to study motor control in birdsong [11]. It is composed of three parts: (1) Newton's second law for the departure x from the prephonatory position of the midpoint of the labium, (2) an expression for the (spatially averaged) interlabial pressure p_g, and (3) an expression for the pressure at the vocal tract input p_i:

$$\dot{x} = y,$$

$$\dot{y} = -\epsilon x - by - cx^2 y - f_0 + p_g, \tag{1}$$

$$p_g = p_s - (a_2/a_1)(p_s - p_i), \tag{2}$$

$$p_i = p_i(x,y). \tag{3}$$

Here ϵ is the linear restitution coefficient, b and c are the linear and nonlinear dissipation coefficients, and f_0 is an external force term, all per unit mass of the labium. p_s stands for the sublabial (bronchial) pressure (all pressures in this work are defined per unit M, with M the mass per unit area of the labium). The entry and exit areas to the labial valve are, respectively,

$$a_1 = 2h(x_{01} + x + \tau y), \tag{4}$$

$$a_2 = 2h(x_{02} + x - \tau y), \tag{5}$$

where h is the labial length (in the dorso-ventral direction), x_{01} and x_{02} are the prephonatory positions of the lower and upper edges of the labium, respectively, and τ is a phenomenological parameter related to flapping motion [22] (see Fig. 2).

In this simple model, the experimentally observed phase difference between upper and lower portions of the labium is imposed through Eqs. (4) and (5)—that is, the flapping motion. On the other hand, more complex models like the two-mass model [15] spontaneously reproduce the experimen-

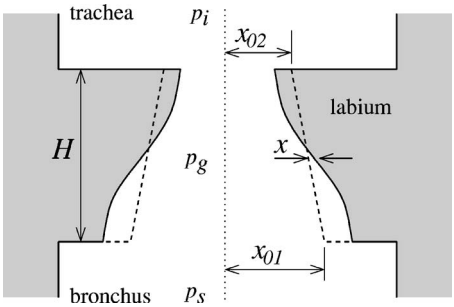

FIG. 2. Geometry of the flapping model for the labia in the avian syrinx, Eqs. (1)–(3). Schematic ventral section of one side of the syrinx (not in scale). The model is symmetric around the dotted line. Dashed line: prephonatory configuration. The actual profile of each labium is approximated by a straight line. Airflow is upwards.

tally observed phase difference, which is the basic mechanism leading to self-oscillating motion [15,22]. However, the two-mass model, for instance, has a phase-space dimensionality of 4; complex dynamics is expected to occur, even considering only one source and disregarding the effect of feedback. The rationale behind using the simple flapping model instead of more complex or realistic models is that it restricts the labial oscillation to a spatially simple mode. In order to study the effect that source-source and source-tract coupling might induce in the dynamics of the labia, we need a system that for low coupling displays simple (two-dimensional) dynamics. The flapping model is a good compromise between a realistic description and simplicity. The final part of our analysis is the design of a set of experiments that would allow us to distinguish between different mechanisms for the generation of complex dynamics.

Note that the dynamics of the labium depends on the pressure at the input of the vocal tract p_i, Eqs. (1) and (2), and this in turn is related to the sound pressure wave being established in the tract. Coupling between source and tract is therefore taken into account in this model by giving a functional form $p_i=p_i(x,y)$ in terms of all the variables describing the flow at the valve exit.

In presence of dissipation, a self-sustained oscillation needs a net transfer of energy to the system to occur. This happens whenever the system is subjected to a force which is in phase with the velocity, such that the work done by the force over the system in a cycle is positive. Note that the vocal valve in flapping motion has a convergent profile (opened to the bronchus) during the opening phase and a divergent profile (opened to the trachea) during the closing phase. Due to this asymmetry in the oscillation cycle, the interlabial pressure p_g is greater during the opening phase than during the closing phase, which allows a net delivery of energy from the airflow to the labial oscillation.

The phenomenological parameter characterizing flapping motion is τ, which stands for the time it takes the surface wave to travel half the labial thickness H. Simple as it is, this model reproduces a wide range of observed song elements with only two basic motor gestures: bronchial pressure and labia tension [10,16].

III. LINEAR APPROXIMATION TO THE GEOMETRICAL FLAPPING FACTOR

The geometrical flapping factor a_2/a_1 in Eq. (2) appeared in Titze's original model as a result of computing the spatial average of the interlabial pressure by means of a modified Bernoulli equation [22]. This geometrical factor is responsible for the net energy transfer from airflow to labial oscillation, leading to self-sustained oscillations. Indeed, when the system is decoupled from the vocal tract ($p_i=0$ or atmospheric pressure), an oscillation starts in a Hopf bifurcation at a value of the sublabial pressure p_s^{Hopf} proportional to $1/\tau$; this threshold value increases indefinitely as $\tau\to 0$—that is, when upper and lower edges of the labium are in phase (not flapping at all).

A first-order Taylor series expansion of the geometrical flapping factor a_2/a_1 in Eq. (2) around the fixed point $(x,y)=(\bar{x},0)$ allows us to identify the mechanism for the loss of stability of the fixed point. We perform the expansion and get

$$\frac{a_2}{a_1} \sim A - Dy + E(x-\bar{x}), \tag{6}$$

where

$$A = \bar{a}_2/\bar{a}_1,$$

$$D = 2h\tau(\bar{a}_1+\bar{a}_2)/\bar{a}_1^2,$$

$$E = 2h(\bar{a}_1-\bar{a}_2)/\bar{a}_1^2,$$

and $\bar{a}_{1,2}=2h(x_{01,02}+\bar{x})$. Note that $E=0$ for a rectangular prephonatory valve. Choosing $x_{01}=x_{02}\equiv x_0$ accordingly without greater detriment of the dynamics, now Eq. (2) simply reads

$$p_g \sim p_s + (Dy - A)(p_s - p_i), \tag{7}$$

with $A=1$, $D=2\tau/(x_0+\bar{x})$, and $E=0$. As expected, the Taylor expansion in Eq. (7) unveils a term in phase with the velocity on the right-hand side of Eq. (1) ($p_s>p_i$, otherwise flow would be inwards). In the case $p_i=0$, the model can be written as

$$\dot{x} = y,$$

$$\dot{y} = -\epsilon x + py - cx^2y - f_0, \tag{8}$$

with $p=Dp_s-b$, which is the standard form of the well-known van der Pol relaxation oscillator [11]. This model allowed a closer relationship of its parameters in terms of physiological parameters [11,12] and has recently been experimentally validated [13].

IV. COUPLING BETWEEN SOURCE AND VOCAL TRACT

When considered, coupling between source and vocal tract has been historically assumed to depend on both the flow at glottal exit $U(t)$ and its time derivative $dU(t)/dt$ through appropriate coupling coefficients [22,24,25]. These coefficients have been associated with the real and imaginary

parts of the vocal tract impedance, typically dependent on nonlocal parameters such as vocal tract length and cross section. This traditional approach relies on the *source-filter separation hypothesis*: the dynamics of the active, nonlinear source (the vocal valve) is independent of the propagation of sound in the passive, linear filter (the vocal tract). However, when source and filter are coupled and let to interact, the complete system is nonlinear and the impedance approach fails to be valid [26]. Indeed, acoustic feedback was shown to be a possible dynamical origin of subharmonic behavior in a model of the human vocal folds [16].

In an interesting work on human phonation by Story and Titze [27], pressure wave propagation in the vocal tract was taken into account, avoiding the use of impedances to model the vocal tract response. However, they restricted the coupling to depend only on $U(t)$ and not on its time derivative.

In order to take into account the effect of acoustic feedback, in this section we will obtain an expression for $p_i=p_i(x,y)$—that is, the source-tract coupling represented in Eq. (3). The general picture of the dynamics of the pressure wave in the vocal tract is that a pressure perturbation is injected by the source at the input of the tract and then travels along it. It is reflected at the end and the interfaces between different sections of the tube and travels back to the base of the trachea, eventually affecting the dynamics of the source some time later. This dynamics can be taken into account through simple boundary conditions as follows, under the hypothesis that the sound wave in the tube is a plane wave.

The pressure at the vocal tract input p_i is composed of two parts: the pressure perturbations $s(t)$ generated by a time-variating flow $U(t)$ injected locally by the valve and a back-propagating sound pressure wave $b(t)$ due to reflections occurring in the tract:

$$p_i(t) = s(t) + b(t - T/2), \tag{9}$$

$$b(t) = -\gamma p_i(t - T/2), \tag{10}$$

where $T/2=L/c$ is the time it takes a sound wave to travel the vocal tract length L at a speed c and γ stands for the reflection coefficient at the end of the tract (which we considered as a uniform tube for simplicity). The source of pressure perturbations $s(t)$ is a function of all the variables describing the dynamics of the labium. Substitution allows us to write Eqs. (9) and (10) more succinctly as

$$p_i(t) = s(t) - \gamma p_i(t - T), \tag{11}$$

with T the round-trip time along the tract. The simple boundary conditions, Eq. (11), assume that the wave propagating along the tract is a plane wave. This hypothesis can be expected to hold in some avian tracts, since we know from the fundamentals of acoustics [18] that a rigid-walled waveguide with a cross-sectional dimension much smaller than the sound wavelength propagates plane waves. A typical songbird's trachea is a tube roughly 1 mm wide, while the wavelength corresponding to a typical frequency of 1000 Hz is 35 cm.

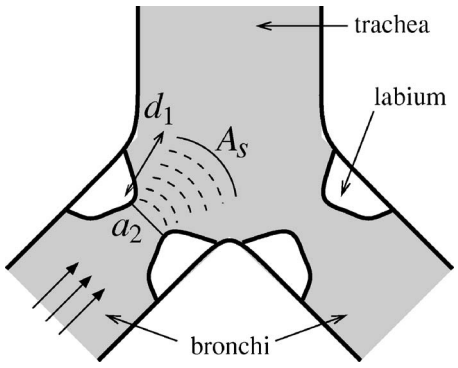

FIG. 3. Coupling between source and tract. Schematic ventral section of the syrinx (not in scale). Airflow driven by air sac pressure is modulated by the airflow-induced oscillation of the labia, injecting a sound pressure wave into the base of the trachea. Dashed lines indicate the region of assumed spherical propagation.

However, we do not expect the sound wave to be a plane wave near the source. There, the emitted sound wave is of a rather diverging nature. In order to get an expression for the pressure perturbations $s(t)$ injected by the valve, for the sake of simplicity we assume that the vocal valve is a local emitter of diverging spherical harmonic waves (see Fig. 3), which are waves of the form

$$s(r,t) = \frac{P_0}{r} e^{i(\omega t - kr)}. \tag{12}$$

The (complex) number P_0 is determined by boundary conditions, which are established at the source [that is, at the very exit of the vocal valve where we know the air particle velocity $v(t)$]. In order to set boundary conditions to determine P_0, we make use of the relationship between s and v for a spherical sound wave, at a distance d_1 from the source. We take d_1 to be much smaller than the wavelength λ, but comparable to the size of the source l according to our local picture. In this way,

$$s(d_1,t) = Z(d_1)v(d_1,t), \tag{13}$$

where $Z=R+i\omega I$ is the complex specific acoustic impedance [18] (redefined in this work per unit M). R and I are termed the specific acoustic resistance and inertance, respectively, and are given by

$$R = \frac{\rho c}{M} \frac{(kd_1)^2}{1 + (kd_1)^2}, \tag{14}$$

$$I = \frac{\rho}{M} \frac{d_1}{1 + (kd_1)^2}, \tag{15}$$

where ρ stands for the air density and c the sound speed [18]. R and I depend on the sound frequency f through the wave number $k=2\pi f/c$. The constant P_0 can be found by evaluating Eq. (12) in $r=d_1$ and equating to Eq. (13). We get

$$P_0 = e^{-i(\omega t - kd_1)} d_1 Z(d_1) v(d_1,t), \tag{16}$$

which does not depend on time, since the particle velocity is also harmonic. By evaluating Eq. (12) at a distance d_2 from

the source (that is, at the base of the trachea where plane wave superposition is valid; see Fig. 3), we finally obtain an expression for the pressure perturbation $s(t)$ at a distance d_2 in terms of the particle velocity $v(t)$ at the source:

$$s(d_2,t) = \frac{d_1}{d_2} Z(d_1) e^{-ik(d_2-d_1)} v(d_1,t). \tag{17}$$

For a spherical harmonic sound disturbance, the particle velocity v is also a harmonic function of time. Thus we can write $\dot{v}=i\omega v$ and rewrite the last expression as

$$s(d_2,t) = \mathcal{R} v(d_1,t) + \mathcal{I} \dot{v}(d_1,t), \tag{18}$$

where we have defined

$$\mathcal{R} = \frac{d_1}{d_2}[R \cos k(d_2-d_1) + \omega I \sin k(d_2-d_1)], \tag{19}$$

$$\mathcal{I} = \frac{d_1}{d_2}\left[I \cos k(d_2-d_1) - \frac{R}{\omega} \sin k(d_2-d_1) \right]. \tag{20}$$

Notice that in general there is a phase difference between pressure s and velocity v in Eq. (18), because of the term in phase with $\dot{v}$. This result states that the phase difference between acoustic pressure and particle velocity is not only due to the spherical geometry of the wave but also to the pressure and velocity being evaluated at different positions. Keeping this in mind, we drop d_1 and d_2 from the arguments of $v(d_1,t)$ and $s(d_2,t)$ from now on and write simply $v(d_1,t) \equiv v(t)$ and $s(d_2,t) \equiv s(t)$. Notice that if the end of the region of spherical propagation is close enough to the region of plane propagation (that is, $d_2-d_1 \ll \lambda$) we can simply write $\mathcal{R} \sim R$ and $\mathcal{I} \sim I$. This is assumed from now on. Thus, Eq. (18) becomes

$$s(t) = R v(t) + I \dot{v}(t). \tag{21}$$

An expression for $v(t)$ in terms of the model variables is needed, in order to relate labial dynamics and pressure. Consistently with our previous hypothesis (spherically diverging flow near the source), we assume that the flow through the valve exit (area a_2) takes a spherical profile, with area A_s at a distance d_1. However, the valve does not radiate in all directions, but only into a fraction of a spherical front. This can be taken into account by writing $A_s = 4\pi d_1^2 q$, with $q < 1$. For flow conservation in the very small region (of size $d_1 \ll \lambda$) between a_2 and A_s let us write

$$v(t) = \frac{a_2(t)}{A_s} v_0 = \frac{2h v_0}{A_s}(x_0 + x - \tau y), \tag{22}$$

where v_0 is an average particle velocity given by Bernouilli, $v_0 = \sqrt{2p_s M/\rho}$. We finally substitute Eq. (22) into Eq. (21), throw the constant term (meaning a constant flow which does not contribute to the acoustic pressure), and redefine the coefficients to get

$$s(t) = \alpha(x - \tau y) + \beta(y - \tau \dot{y}), \tag{23}$$

which together with Eq. (11) constitutes an expression for the pressure $p_i(t)$ at the input of the trachea in terms of the valve variables. We have defined the coupling coefficients

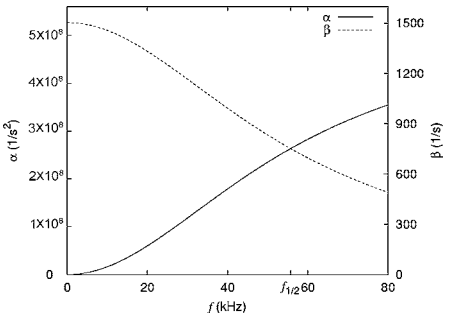

FIG. 4. Coupling parameters α and β [Eqs. (24) and (25)], as a function of sound frequency f. At low frequencies the only surviving parameter is β. The coupling in this case is said to be mainly *inertive*; that is, sound pressure and particle velocity are almost $\pi/2$ out of phase. On the contrary, at high frequencies the only surviving parameter is α and the coupling is *resistive* (sound pressure in phase with particle speed). Both parameters take their corresponding half-maximum values at the crossover frequency $f_{1/2} = c/(2\pi d_1) \sim 55$ kHz. Parameter values are those of Table I throughout this work, unless otherwise specified.

$$\alpha = 2h \frac{v_0}{A_s} R, \tag{24}$$

$$\beta = 2h \frac{v_0}{A_s} I, \tag{25}$$

which depend on the sound frequency f through R and I [Eqs. (14) and (15)]. A plot of α and β as functions of sound frequency f is displayed in Fig. 4. Notice that α and β are just a scaling of R and I, respectively. α takes the value zero at $f=0$ and monotonically increases to a maximum value of $2h(v_0/A_s)(\rho c/M)$ as frequency goes to infinity. β starts at $f=0$, taking its maximum value $2h(v_0/A_s)(\rho d_1/M)$, and monotonically goes to zero as the frequency goes to infinity. Parameters α and β are not independent quantities; they are related by

$$\alpha = F\beta, \tag{26}$$

where $F = 4\pi^2 f^2 d_1/c$.

At low enough frequencies, coupling between source and tract is mostly inertive, which means that the acoustic pressure is proportional to the time derivative of the particle velocity (the only surviving coefficient is β). However, as frequency is increased both terms contribute to $s(t)$. Eventually, as frequency is increased even more, the coupling becomes mostly resistive; that is, the acoustic pressure is in phase with particle velocity. The crossover frequency (the frequency at which both coefficients take half their corresponding maximum value) is

$$f_{1/2} = c/(2\pi d_1). \tag{27}$$

In the case of considering two sources coupled to the tract, Eq. (23) should be modified in order to account for the pressure perturbations induced by both sources. This can be done by simply adding the contributions from both sources, labeled l (left) and r (right):

TABLE I. Standard set of parameter values throughout this work, unless otherwise specified. Parameter values are the same for both sources, unless otherwise specified.

$\epsilon=3\times10^{8}$	(s^{-2})
$b=2\times10^{4}$	(s^{-1})
$c=2\times10^{8}$	(s^{-1} cm^{-2})
$f_0=4.9\times10^{4}$	(cm s^{-2})
$p_s=6\times10^{6}$	(cm s^{-2})
$x_0=0.04$	(cm)
$h=0.1$	(cm)
$\tau=1\times10^{-4}$	(s)
$M=5\times10^{-3}$	(g cm^{-2})
$A=1.0$	
$D=5\times10^{-3}$	(s cm^{-1})
$\alpha=1.2\times10^{6}$	(s^{-2})
$\beta=1.5\times10^{3}$	(s^{-1})
$f=2500$	(Hz)
$d_1=0.1$	(cm)
$q=0.175$	
$L=2.0$	(cm)
$\gamma=0.9$	
$c_a=3.5\times10^{4}$	(cm s^{-1})
$c_H=6.09\times10^{4}$	(cm s^{-1})
$\rho_a=0.00114$	(g cm^{-3})
$\rho_H=0.00034$	(g cm^{-3})

$$s(t)=s_l(t)+s_r(t)=\alpha_l(x_l-\tau_l y_l)+\beta_l(y_l-\tau_l\dot{y}_l)+\alpha_r(x_r-\tau_r y_r)+\beta_r(y_r-\tau_r\dot{y}_r). \tag{28}$$

V. COMPLETE MODEL

The complete model for two sources coupled to a tract with feedback is assembled by gathering Eqs. (1), (7), (11), and (28). Notice that Eq. (28) introduces acceleration terms on the right-hand side of Newton's law [Eq. (1)]; they are inherited directly from the flapping motion and reflect the fact that flow exiting the valve is not in phase with x. These terms make the system lose the explicit form $\dot{\mathbf{x}}=\mathbf{F}(\mathbf{x})$, which prevents us from using a standard Runge-Kutta numerical integrator. In addition, an algebraic equation with time delay is involved. However, the system can be put in a form amenable to integration by means of a Runge-Kutta method. In order to do so, we consider for the sake of clarity first the case of one source coupled to a vocal tract and then the case of two sources coupled to a vocal tract.

A. One source

Putting together Eqs. (1), (7), (11), and (23), the complete model for one source coupled to a tract reads, so far,

$$\dot{x}=y,$$

$$\dot{y}=f(x,y)+p_g, \tag{29}$$

$$f(x,y)=-\epsilon x-by-cx^2y-f_0, \tag{30}$$

$$p_g=p_s+(Dy-A)(p_s-p_i), \tag{31}$$

$$p_i(t)=\alpha(x-\tau y)+\beta(y-\tau\dot{y})-\gamma p_i(t-T), \tag{32}$$

which is not in explicit form $\dot{\mathbf{x}}=\mathbf{F}(\mathbf{x})$ because of the term with $\dot{y}$ in Eq. (32). To put the system in a form useful for Runge-Kutta integration we first segregate the acceleration term in Eq. (32) and write

$$\dot{x}=y,$$

$$\dot{y}=f(x,y)+\tilde{p}_g+(Dy-A)\beta\tau\dot{y}, \tag{33}$$

$$f(x,y)=-\epsilon x-by-cx^2y-f_0, \tag{34}$$

$$\tilde{p}_g=p_s+(Dy-A)(p_s-\tilde{p}_i), \tag{35}$$

$$\tilde{p}_i(t)=\alpha(x-\tau y)+\beta y-\gamma p_i(t-T), \tag{36}$$

$$p_i(t)=\alpha(x-\tau y)+\beta(y-\tau\dot{y})-\gamma p_i(t-T). \tag{37}$$

Notice the definition of $\tilde{p}_g$ and especially that of $\tilde{p}_i$ (in contrast to those of p_g and p_i). We then solve for $\dot{y}$ in Eq. (33):

$$\dot{x}=y,$$

$$\dot{y}=[f(x,y)+\tilde{p}_g][1-(Dy-A)\beta\tau]^{-1}, \tag{38}$$

$$f(x,y)=-\epsilon x-by-cx^2y-f_0, \tag{39}$$

$$\tilde{p}_g=p_s+(Dy-A)(p_s-\tilde{p}_i), \tag{40}$$

$$\tilde{p}_i(t)=\alpha(x-\tau y)+\beta y-\gamma p_i(t-T), \tag{41}$$

$$p_i(t)=\alpha(x-\tau y)+\beta(y-\tau\dot{y})-\gamma p_i(t-T). \tag{42}$$

Now we can apply a Runge-Kutta method to integrate the system. Note the difference between the argument of p_i in Eq. (41) and that in Eq. (42). This difference allows us to numerically solve this system as follows: first integrate Eq. (38) at time t along with definitions (39), (40), and (41), for a given $p_i(t-T)$ (either as an initial condition or computed previously); then compute p_i with Eq. (42) to be used later at the instant $t+T$. This is done by keeping track of the values of p_i at each time step from $t-T$ to t (an interval of length T before t). Initial conditions for this system are $x(t=0)=x_0$, $y(t=0)=y_0$, and $p_i(t\in[-T,0])=p_{i0}(t)$. Note that p_i must be initially defined in an interval of length T.

B. Two sources

We now consider the Oscine case of two sources coupled to a tract. Sources are labeled l (left) and r (right). The two-source case is easily obtained from the one-source case. We

write Newton's law [Eq. (29)], the definition of $f(x,y)$ [Eq. (30)], and the interlabial pressure p_g [Eq. (31)] for each source, plus Eq. (28), which is common to both sources:

$$\dot{x}_l = y_l,$$

$$\dot{y}_l = f_l(x_l,y_l) + p_{gl}, \tag{43}$$

$$\dot{x}_r = y_r,$$

$$\dot{y}_r = f_r(x_r,y_r) + p_{gr}, \tag{44}$$

$$f_j(x_j,y_j) = -\epsilon_j x_j - b_j y_j - c_j x_j^2 y_j - f_{0j}, \tag{45}$$

$$p_{gj} = p_s + (D_j y_j - A_j)(p_s - p_i), \tag{46}$$

$$p_i(t) = \alpha_l(x_l - \tau_l y_l) + \beta_l(y_l - \tau_l \dot{y}_l) + \alpha_r(x_r - \tau_r y_r) + \beta_r(y_r - \tau_r \dot{y}_r) - \gamma p_i(t-T) \tag{47}$$

$(j=l,r)$. Notice that p_i is formed with the contribution from each source, plus the reflected wave. Pressure p_i is common to both sources (because it is defined at the base of the trachea), as well as the sublabial pressure p_s which is associated to the air sac pressure.

Following steps analogous to those of the previous subsection, we segregate the acceleration terms in Eq. (47) and write

$$\dot{x}_l = y_l,$$

$$\dot{y}_l = f_l(x_l,y_l) + \tilde{p}_{gl} + (D_l y_l - A_l)(\beta_l \tau_l \dot{y}_l + \beta_r \tau_r \dot{y}_r), \tag{48}$$

$$\dot{x}_r = y_r,$$

$$\dot{y}_r = f_r(x_r,y_r) + \tilde{p}_{gr} + (D_r y_r - A_r)(\beta_l \tau_l \dot{y}_l + \beta_r \tau_r \dot{y}_r), \tag{49}$$

$$f_j(x_j,y_j) = -\epsilon_j x_j - b_j y_j - c_j x_j^2 y_j - f_{0j}, \tag{50}$$

$$\tilde{p}_{gj} = p_s + (D_j y_j - A_j)(p_s - \tilde{p}_i), \tag{51}$$

$$\tilde{p}_i(t) = \alpha_l(x_l - \tau_l y_l) + \beta_l y_l + \alpha_r(x_r - \tau_r y_r) + \beta_r y_r - \gamma p_i(t-T), \tag{52}$$

$$p_i(t) = \alpha_l(x_l - \tau_l y_l) + \beta_l(y_l - \tau_l \dot{y}_l) + \alpha_r(x_r - \tau_r y_r) + \beta_r(y_r - \tau_r \dot{y}_r) - \gamma p_i(t-T). \tag{53}$$

Notice again the definition of $\tilde{p}_{gj}$ and $\tilde{p}_i$, analogous to those in the previous subsection. Now Eqs. (48) and (49) are two coupled, linear equations in $\dot{y}_l$ and $\dot{y}_r$. By solving for $\dot{y}_r$ in Eq. (49) and substituting into Eq. (48), we get an expression for $\dot{y}_l$:

$$\dot{y}_l = \{[1-(D_r y_r - A_r)\beta_r \tau_r][f_l(x_l,y_l) + \tilde{p}_{gl}] + (D_l y_l - A_l)\beta_r \tau_r [f_r(x_r,y_r) + \tilde{p}_{gr}]\} \times [1-(D_l y_l - A_l)\beta_l \tau_l - (D_r y_r - A_r)\beta_r \tau_r]^{-1}. \tag{54}$$

A similar result (interchanging labels $l \leftrightarrow r$) stands for $\dot{y}_r$. With this, we can set our system in a form analogous to that of the previous subsection:

$$\dot{x}_l = y_l,$$

$$\dot{y}_l = \{[1-(D_r y_r - A_r)\beta_r \tau_r][f_l(x_l,y_l) + \tilde{p}_{gl}] + (D_l y_l - A_l)\beta_r \tau_r [f_r(x_r,y_r) + \tilde{p}_{gr}]\} \times [1-(D_l y_l - A_l)\beta_l \tau_l - (D_r y_r - A_r)\beta_r \tau_r]^{-1}, \tag{55}$$

$$\dot{x}_r = y_r,$$

$$\dot{y}_r = \{[1-(D_l y_l - A_l)\beta_l \tau_l][f_r(x_r,y_r) + \tilde{p}_{gr}] + (D_r y_r - A_r)\beta_l \tau_l [f_l(x_l,y_l) + \tilde{p}_{gl}]\} \times [1-(D_l y_l - A_l)\beta_l \tau_l - (D_r y_r - A_r)\beta_r \tau_r]^{-1}, \tag{56}$$

$$f_j(x_j,y_j) = -\epsilon_j x_j - b_j y_j - c_j x_j^2 y_j - f_{0j}, \tag{57}$$

$$\tilde{p}_{gj} = p_s + (D_j y_j - A_j)(p_s - \tilde{p}_i), \tag{58}$$

$$\tilde{p}_i(t) = \alpha_l(x_l - \tau_l y_l) + \beta_l y_l + \alpha_r(x_r - \tau_r y_r) + \beta_r y_r - \gamma p_i(t-T), \tag{59}$$

$$p_i(t) = \alpha_l(x_l - \tau_l y_l) + \beta_l(y_l - \tau_l \dot{y}_l) + \alpha_r(x_r - \tau_r y_r) + \beta_r(y_r - \tau_r \dot{y}_r) - \gamma p_i(t-T). \tag{60}$$

Notice again the difference between the argument of p_i in Eq. (59) and that in Eq. (60). The comments following Eqs. (38)–(42) regarding the numerical integration of this system are also valid here.

C. Small coupling approximation

One last approximation is worthwhile, in order to get a much simpler form for our system. We would like to know specifically whether it is possible to throw the terms $(D_j y_j - A_j)\beta_j \tau_j$ in front of 1 in the denominators of Eqs. (55) and (56).

There are often several ways to nondimensionalize an equation. In order to make the correct approximation we proceed as in Ref. [28]. After noting that A_j is already nondimensional and $A_j \sim 1$ even for a nonrectangular prephonatory glotis [Eq. (6)], nondimensionalization of the variables t and x and the equations themselves make all variables and derivatives have order 1, and lead us to

$$(D_j y_j - A_j)\beta_j \tau_j \ll 1 \quad \text{if} \quad \beta_j \ll \tau_j^{-1} \tag{61}$$

$(j=l,r)$. This approximation can be interpreted in several ways. The most direct interpretation is roughly that of small coupling: the approximation is valid only if β_j is sufficiently small, which at fixed frequency depends on anatomical and acoustic parameters. A second interpretation is related to the phase difference between upper and lower portions of the labium in the flapping motion, which is directly governed by the value of τ_j [recall Eqs. (4) and (5)]. From this viewpoint, the condition is satisfied for small values of τ_j—that is, a

small phase difference. A third interpretation is based on the behavior of β_j as a function of frequency. As β_j decreases with frequency (Fig. 4), the condition is fulfilled for frequency values large enough.

Note that this approximation allows us to neglect in addition the cross terms in the numerators of Eqs. (55) and (56). In the numerator of Eq. (55), for example, we are referring specifically to

$$(D_r y_r - A_r)\beta_r \tau_r \ll 1,$$

$$(D_l y_l - A_l)\beta_r \tau_r [f_r(x_r, y_r) + \tilde{p}_{gr}] \ll f_l(x_l, y_l) + \tilde{p}_{gl}.$$

The approximated system is finally

$$\dot{x}_l = y_l,$$

$$\dot{y}_l = f_l(x_l, y_l) + \tilde{p}_{gl}, \tag{62}$$

$$\dot{x}_r = y_r,$$

$$\dot{y}_r = f_r(x_r, y_r) + \tilde{p}_{gr}, \tag{63}$$

$$f_j(x_j, y_j) = -\epsilon_j x_j - b_j y_j - c_j x_j^2 y_j - f_{0j}, \tag{64}$$

$$\tilde{p}_{gj} = p_s + (D_j y_j - A_j)(p_s - \tilde{p}_i), \tag{65}$$

$$\tilde{p}_i(t) = \alpha_l(x_l - \tau_l y_l) + \beta_l y_l + \alpha_r(x_r - \tau_r y_r) + \beta_r y_r - \gamma p_i(t - T), \tag{66}$$

$$p_i(t) = \alpha_l(x_l - \tau_l y_l) + \beta_l(y_l - \tau_l \dot{y}_l) + \alpha_r(x_r - \tau_r y_r) + \beta_r(y_r - \tau_r \dot{y}_r) - \gamma p_i(t - T) \tag{67}$$

$(j = l, r)$, which is the main result of this work. Note that by setting the coupling parameters of the second source to zero, the one-source model is recovered [Eqs. (38)–(42), in the small coupling approximation]. Furthermore, by setting also the coupling parameters of the first source to zero, the single, isolated source is recovered [Eqs. (1)–(3), with $p_i = 0$]. As discussed in the Introduction, the isolated, single source is a two-dimensional (2D) dynamical system, and for that reason it cannot show complex dynamics by itself. That is why we chose the flapping model to describe labial motion. In this way the possible origins of complexity are separated (intrinsic dynamics of the source and coupling effects), which allows us to study the effect of feedback on the motion of one source, as well as the effect of acoustically coupling the two sources.

VI. SIMULATIONS AND THEORETICAL PREDICTIONS

A. Simulations

The model developed in this work for two sources acoustically coupled to a tract with feedback [Eqs. (62)–(67)], presents an extremely rich dynamics. Preliminary observations show periodic and nonperiodic oscillatory solutions and period-doubling bifurcations (see below; a detailed analysis of the solutions of one and two coupled sources will be published elsewhere).

As an illustration of the richness of solutions, in this work we show simulations corresponding to (a) only one source being active and feedback is considered and (b) both sources being active and feedback is not considered. The first case occurs naturally in Oscine birds, since they have the capability of actively silencing one side of the syrinx by means of the gating muscles syringealis dorsalis and tracheobronchialis dorsalis [20], which are lateralized [5]. In our model, a configuration with only one active source is simply achieved by setting f_0 of the second source (a parameter related to the action of gating muscles [11]) to a sufficiently large value. However, the second case might seem, physiologically speaking, somewhat unattainable. Although the silencing of one source is a well-established vocal maneuver in Oscines, the choice of whether feedback is present or not is hardly under the bird's control. The reason for separating cases (a) and (b) is dynamical in nature. As stated in Sec. II, we want to separate the sources of complexity and show that feedback alone is a possible dynamical origin of complex spectra in sonograms, as well as source-source acoustic coupling alone.

Simulations of only one source active with feedback are displayed in Fig. 5. Two possible vocal maneuvers are simulated: (a) varying ϵ, which is interpreted as varying the tension of the vS muscle and leads to a varying vocalization frequency, and (b) varying p_s, which is interpreted as varying air sac pressure and leads to a varying sound intensity. Interpretation of these vocal maneuvers was established in previous works [10,11]. A third simulation is also shown, where we vary β [and α accordingly; see Eq. (26)] to study the effect of different configurations of the valve-tract interphase in the dynamics of the source. Recall that β depends on anatomical parameters like d_1 [Eq. (25)], which may be interpreted as a measure of the distance between the vocal valve and the base of the trachea.

Period-doubling and period-halving bifurcations are evident in Fig. 5. Notice that feedback is the only dynamical origin of this rich behavior, because the active source is modeled as a 2D system; it cannot show complex behavior by its own. Indeed, for low coupling the dynamics of the system is still two dimensional.

Let us now turn our attention to the case of two coupled sources without feedback. The effect of feedback in our model can be easily suppressed by setting $\gamma = 0$. The subharmonic behavior of the model in this case is illustrated in Fig. 6. Notice that there are frequencies appearing when both sources are simultaneously active and acoustically coupled [panel (a)] that are not present in the spectra of the isolated sources [panels (b) and (c)]. We isolated source $l(r)$ from the other source by setting $\alpha_r = 0$ and $\beta_r = 0$ ($\alpha_l = 0$ and $\beta_l = 0$), all other parameters being kept the same as in Fig. 6(a).

The effect of feedback was turned off on purpose by setting $\gamma = 0$; hence acoustic coupling between the two sound sources is the only dynamical origin of the subharmonic frequencies displayed in Fig. 6(a). The fact that the sources do not display complex dynamics by themselves is illustrated in Figs. 6(b) and 6(c). The spectra of the isolated sources display a fundamental frequency plus harmonic overtones.

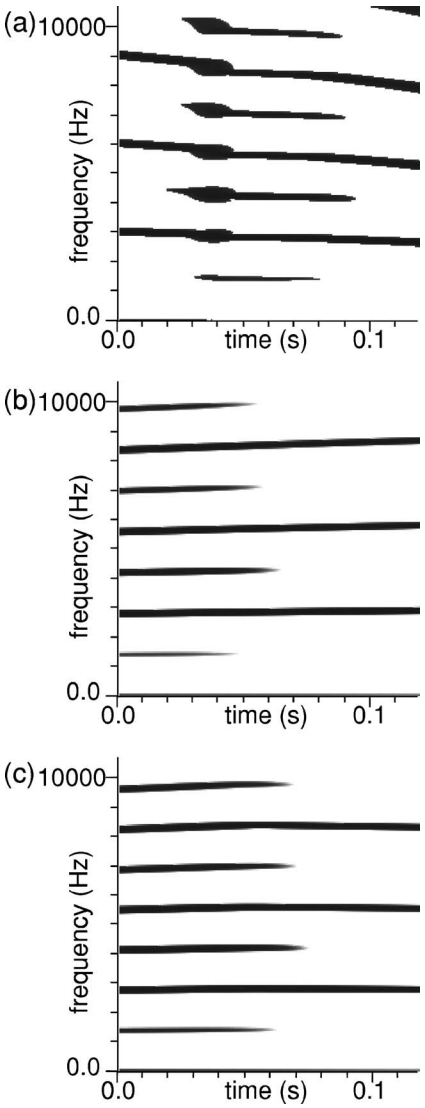

FIG. 5. Simulated vocal maneuvers for the model [Eqs. (62)–(67)], with only one source active and feedback (the second source is silenced by increasing ipsilateral f_0 to a sufficiently large value). Sonograms of the acoustic pressure p_i are shown here and in the following figures. Parameter values are those of Table I throughout this work, unless otherwise specified. (a) Varying ϵ. Appearance and disappearance of subharmonic frequencies are evident as ϵ is continuously decreased from 3.6×10^8 s^{-2} to 2.6×10^8 s^{-2}. (b) Varying p_s. Subharmonic frequencies disappear as p_s is continuously decreased from 6.2×10^6 cm s^{-2} to 4.2×10^6 cm s^{-2}. (c) Varying β [and α, according to Eq. (26)]. Subharmonic frequencies disappear as β is continuously decreased from 1900 s^{-1} to 900 s^{-1}.

B. Predictions

A way to explore and validate this model consists in studying how the dynamics can be affected as certain parameters are changed. In particular, the density of the atmosphere in which this model operates can be changed. Our model predicts that qualitatively different scenarios will be obtained as the density of the atmosphere changes, if the source of subharmonicity is the acoustic interaction between source and tract or if it is high-order modes of labial vibration. In

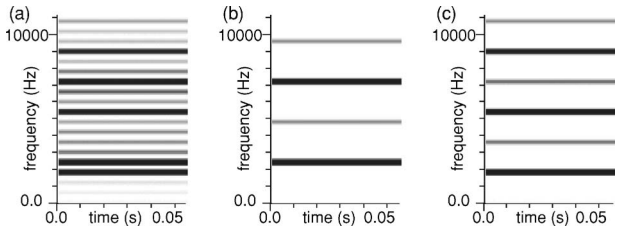

FIG. 6. Simulation of the model for two coupled sources [Eqs. (62)–(67)], without feedback (feedback is suppressed by setting $\gamma=0$). The restitution coefficients are set in this figure to $\epsilon_l=2.4\times10^8$ s^{-2} and $\epsilon_r=1.4\times10^8$ s^{-2}. Other parameter values are those of Table I. (a) Sonogram of the acoustic pressure p_i for the two coupled sources. Notice the two dark strokes around 2000 Hz. Every frequency in this sonogram is a multiple of the difference between these two frequencies. (b),(c) Sonogram of the left and right isolated sources, respectively. Parameter values are exactly the same as in (a), except the coupling coefficients: α_r and β_r are set to zero when source l is considered alone (isolated from source r), and conversely α_l and β_l are set to zero when the source r is considered alone. Notice that the sonogram in (a) is not just the superposition of the sonograms of the isolated sources, but has in addition several other frequencies that are sums and differences of multiples of the fundamental frequencies of the isolated sources.

the following we will show that the coupling parameters α and β should change appreciably when the bird is immersed in a heliox atmosphere, in which nitrogen, comprising 80% of ordinary air, is replaced with the less dense helium. Helium density is one-eighth that of nitrogen, so heliox has a density 30% that of ordinary air. Sound speed in heliox is 74% greater than in air [29,30].

Experiments with singing birds in a heliox atmosphere were performed in the past. Heliox experiments were devised to show that some birds actively coordinate the passive filter characteristics of their vocal tracts with the output of the syrinx [30]. There it was shown that the tract does shape the spectral characteristics of the syringeal output, but has little influence on the vibration of the membranes. Heliox was also used to test the "whistle hypothesis" in doves [8]. In this scenario, sound is presumably generated when *eolic noise* (turbulence) is induced by forcing the airflow through a constriction in the syrinx. The fundamental frequency of the emitted sound is determined by the resonances of the tract that stabilize the acoustic disturbance. The experiment indicated that also in these birds vocalizations are not produced as in a whistle, but are the result of membrane vibration. Analogous results were obtained for the psittacine budgerigar [9].

The expected outcome of each of the above discussed heliox experiments was either a change in the fundamental frequency of the vocalization in the same proportion sound velocity changes or a change only in the resonances of the tract with little change in the fundamental frequency. However, in this section we will show that other possible results can be expected from a heliox experiment when the source is acoustically coupled to the tract. These results are different from those expected in the two traditionally considered high-coupling scenarios, where the fundamental frequency changes in much the same proportion as the resonances of

the tube do: a whistle [8,9,30] or a pressure-controlled vibrating valve [9,25] like that of woodwinds or brasses.

In the following we will make explicit the dependence of the coupling coefficients α and β on the acoustic parameters ρ (air density) and c (sound speed). Recall first the definition of the specific acoustic inertance I, Eq. (15). We can write

$$I = \frac{\rho}{M}\frac{d_1}{1+(kd_1)^2} \sim \rho g(f), \tag{68}$$

with

$$g(f) = \frac{1}{1+(kd_1)^2}, \quad k = 2\pi f/c.$$

Note that the function $g(f)$ depends on c through the wave number k. However, $g(f)$ takes the value 1 with zero derivative at $f=0$ and decreases to zero as frequency tends to infinity, taking its half-maximum value at $f_{1/2}=c/(2\pi d_1)$ [Eq. (27)]. At low frequencies $g(f)\sim 1$ and it changes very little with c when ordinary air is changed to heliox; that is why we write $g(f)$. With Eq. (68) we can write the coupling parameter β, Eq. (25):

$$\beta = 2h\frac{v_0}{A_s} I \sim \rho^{1/2} g(f), \tag{69}$$

where we have used that $v_0 \sim \rho^{-1/2}$ [see the definition following Eq. (22)]. Recall now the relationship between α and β, Eq. (26):

$$\alpha = 4\pi^2 f^2 d_1 c^{-1} \beta \sim \rho^{1/2} c^{-1} g(f). \tag{70}$$

So far, Eqs. (69) and (70) give us the explicit dependence of β and α, respectively, on the acoustic parameters ρ and c. Keeping in mind the behavior of $g(f)$ discussed above, we can say that when changing from ordinary air (a) to heliox (H) the coupling coefficients should scale approximately as

$$\alpha_H \sim \frac{c_a}{c_H}\left(\frac{\rho_a}{\rho_H}\right)^{-1/2} \alpha_a \sim 0.31\alpha_a, \tag{71}$$

$$\beta_H \sim \left(\frac{\rho_a}{\rho_H}\right)^{-1/2} \beta_a \sim 0.55\beta_a. \tag{72}$$

This result allows us to predict that noticeable changes may occur in the sonograms when air is replaced by heliox. In Fig. 7(a) we show a simulation of the model, Eqs. (62)–(67), for only one source active with feedback. Parameter p_s is continuously decreased exactly as in Fig. 5(b). In the left inset (ordinary air), subharmonic behavior is evident at the beginning of the sonogram. Subharmonic frequencies disappear in a period-halving bifurcation around 0.05 s when p_s goes below the bifurcation value. When air is replaced by heliox (right inset), the subharmonic frequencies are not present.

It is worth noticing that, contrary to what would be expected in other coupled vibrating-valve mechanisms like a trumpet, a trombone, or woodwinds [9], the fundamental frequency almost does not change from air to heliox [see Fig. 7(a): nonhalved fundamental frequency in left inset versus fundamental frequency in right inset]. Nonetheless, coupling is at work here, since appreciable changes in the sonogram are evident.

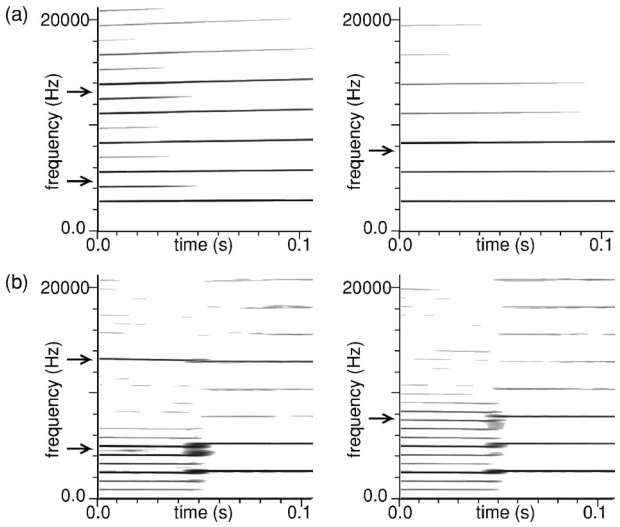

FIG. 7. Predicted sonograms in heliox experiments. (a) Simulation of the model [Eqs. (62)–(67)], with only one source active with feedback. Parameter p_s is continuously decreased exactly as in Fig. 5(b) (a linear scale for the intensity is used here, to allow discrimination of tract resonances). Left inset: ordinary air, where subharmonic frequencies are evident at the beginning of the sonogram. A period-halving bifurcation takes place around 0.05 s. Right inset: same maneuver under heliox. Subharmonic behavior is not present. Not considering the bifurcation, it is worth noticing that, although source and tract are coupled, the fundamental frequency almost does not change from air to heliox. (b) Simulation of an asymmetric two-mass model [15], without coupling to a tract [the time series is filtered afterwards, following the prescription of Eqs. (11)]. Left-side masses and elastic coefficients are 52% those of the right side. The sublabial pressure is continuously decreased in a way analogous to that in (a). Left inset: ordinary air. An inverse period-tripling bifurcation occurs around 0.05 s. Right inset: same maneuver under heliox. The subharmonic behavior is still present. The only evident change is the increase in the resonances of the tract. Arrows approximately indicate vocal tract resonances: 4375 Hz and 13125 Hz (ordinary air) and 7612 Hz (heliox). Higher resonances lie beyond 20 000 Hz. Parameter values are those of Table I throughout this work, unless otherwise specified.

On the contrary, a heliox experiment will show little difference if the dynamical origin of subharmonic frequencies in the sonogram is the appearance of high-order modes of tissue vibration. In Fig. 7(b) we show a simulation of an asymmetric two-mass model without coupling to a tract, which does not depend on air density or sound speed [15]. A vocal maneuver similar to that of Fig. 7(a) is performed: sublabial pressure is continuously decreased in order to show an inverse period-tripling bifurcation. The subharmonic frequencies are always present either in air or in heliox. We want to point out that the only differences between left and right insets in Fig. 7 are the values of air density and sound speed.

However, we will be in a position of saying something about the effect of acoustic feedback only in case a difference like the one shown in Fig. 7(a) is found. Given a bird, it may be the case that the changes in density and sound speed

achieved by using heliox are not enough to lower the coupling coefficients to values so that the effect of acoustic feedback is suppressed. Different ways to modify acoustic feedback should be attempted in that case—for example, changing the vocal tract length by means of a cannula inserted at any position in the trachea (posible effects of a tracheotomy are discussed in Ref. [17]) or other mechanical or anatomical modifications.

VII. CONCLUSIONS

In this work we presented a model for the production of sound in the Oscine syrinx, taking into account both source-source and source-tract acoustic interactions. This model let us study complex birdsong phenomena in which the vocal sources are not independent of each other or the traditionally assumed source-filter separation hypothesis does not hold. We showed that there might be mechanisms, other than intrinsic nonlinearity of the labium, underlying complex features in sonograms. In the absence of contrary experimental evidence, the source-filter acoustic interaction must be taken into account as a possible dynamical origin of complexity in birdsong.

Based on theoretical considerations, we proposed simple heliox experiments that would allow us to discriminate among possible origins of complexity in sonograms. Our model allows us to predict that subharmonic frequencies due to source-tract coupling might dissapear from a sonogram, or at least be greatly reduced, when the recording is made in a heliox atmosphere. On the other hand, subharmonic frequencies recorded in ordinary air would not be affected by heliox, if they were due to intrinsic nonlinearity of the labium.

ACKNOWLEDGMENTS

This work was financially supported by University of Buenos Aires, Consejo Nacional de Investigaciones Científicas y Técnicas (Argentina), and NIH.

[1] M. S. Brainard and A. J. Doupe, Nature (London) **417**, 351 (2002).
[2] E. D. Jarvis, Ann. N.Y. Acad. Sci. **1016**, 749 (2004).
[3] M. S. Fee, B. Shraiman, B. Peseran, and P. P. Mitra, Nature (London) **395**, 67 (1998).
[4] F. Goller and O. N. Larsen, J. Comp. Physiol., A **188**, 841 (2002).
[5] F. Goller and R. A. Suthers, Nature (London) **373**, 63 (1995).
[6] R. A. Suthers, Nature (London) **347**, 473 (1990).
[7] F. Goller and O. N. Larsen, Proc. Natl. Acad. Sci. U.S.A. **94**, 14787 (1997).
[8] M. R. Ballintijn and C. ten Cate, J. Exp. Biol. **201**, 1637 (1998).
[9] E. F. Brittan-Powell, R. J. Dooling, O. N. Larsen, and J. T. Heaton, J. Acoust. Soc. Am. **101**, 578 (1997).
[10] T. J. Gardner, G. Cechi, M. Magnasco, R. Laje, and G. B. Mindlin, Phys. Rev. Lett. **87**, 208101 (2001).
[11] R. Laje, T. J. Gardner, and G. B. Mindlin, Phys. Rev. E **65**, 051921 (2002).
[12] R. A. Suthers and D. Margoliash, Curr. Opin. Neurobiol. **12**, 684 (2002).
[13] G. B. Mindlin, T. J. Gardner, F. Goller, and R. Suthers, Phys. Rev. E **68**, 041908 (2003).
[14] R. Straneck, *Canto de las Aves Pampeanas I* (LOLA, Buenos Aires, 1990).
[15] I. Steinecke and H. Herzel, J. Acoust. Soc. Am. **97**, 1874 (1995).
[16] R. Laje, T. J. Gardner, and G. B. Mindlin, Phys. Rev. E **64**, 056201 (2001).
[17] G. J. L. Beckers, R. A. Suthers, and C. ten Cate, Proc. Natl. Acad. Sci. U.S.A. **100**, 7372 (2003).
[18] L. E. Kinsler, A. R. Frey, A. B. Coppens, and J. V. Sanders, *Fundamentals of Acoustics* (Wiley, New York, 1982).
[19] S. Nowicki and R. R. Capranica, Science **231**, 1297 (1986).
[20] F. Goller and R. A. Suthers, J. Neurophysiol. **75**, 867 (1996).
[21] O. N. Larsen and F. Goller, Proc. R. Soc. London, Ser. B **266**, 1609 (1999).
[22] I. R. Titze, J. Acoust. Soc. Am. **83**, 1536 (1988).
[23] J. G. Švec, H. K. Schutte, and D. G. Miller, J. Speech Hear. Res. **39**, 135 (1996).
[24] I. R. Titze and B. H. Story, J. Acoust. Soc. Am. **101**, 2234 (1997).
[25] N. H. Fletcher and A. Tarnopolsky, J. Acoust. Soc. Am. **105**, 35 (1999).
[26] G. B. Mindlin and R. Laje, *The Physics of Birdsong* (Springer-Verlag, Berlin, 2005).
[27] B. H. Story and I. R. Titze, J. Acoust. Soc. Am. **97**, 1249 (1995).
[28] S. H. Strogatz, *Nonlinear Dynamics and Chaos* (Perseus, Cambridge, England, 1994).
[29] *American Institute of Physics Handbook*, 2nd. ed., edited by D. E. Grey (McGraw-Hill, New York, 1963).
[30] S. Nowicki, Nature (London) **325**, 53 (1987).